Journal of Geophysical Research: Space Physics

RESEARCH ARTICLE
10.1029/2018JA025645

Key Points:
- Principal component analysis is performed separately on the dayside and nightside portions of field-aligned current maps measured by AMPERE
- We determine the timescales of dayside and nightside response to changes in the polarity of IMF B_Z and By and the occurrence of substorms
- Nightside responses are delayed, interpreted in terms of the substorm cycle and the induction of a B_Y component in the magnetotail

Correspondence to:
S. E. Milan,
steve.milan@le.ac.uk

Citation:
Milan, S. E., Carter, J. A., Sangha, H., Laundal, K. M., Østgaard, N., Tenfjord, P., et al. (2018). Timescales of dayside and nightside field-aligned current response to changes in solar wind-magnetosphere coupling. *Journal of Geophysical Research: Space Physics*, *123*. https://doi.org/10.1029/2018JA025645

Received 4 MAY 2018
Accepted 14 JUL 2018
Accepted article online 23 JUL 2018

Timescales of Dayside and Nightside Field-Aligned Current Response to Changes in Solar Wind-Magnetosphere Coupling

Stephen E. Milan[1,2], Jennifer Alyson Carter[1], Harneet Sangha[1], Karl M. Laundal[2], Nikolai Østgaard[2], Paul Tenfjord[2], Jone Peter Reistad[2], Kristian Snekvik[2], John C Coxon[3], Haje Korth[4], and Brian J. Anderson[4]

[1]Department of Physics and Astronomy, University of Leicester, Leicester, UK, [2]Birkeland Centre for Space Science, University of Bergen, Bergen, Norway, [3]Department of Physics and Astronomy, University of Southampton, Southampton, UK, [4]The Johns Hopkins University Applied Physics Laboratory, Laurel, MD, USA

Abstract Principal component analysis is performed on Birkeland or field-aligned current (FAC) measurements from the Active Magnetosphere and Planetary Electrodynamics Response Experiment, to determine the response of dayside and nightside FACs to reversals in the orientation of the interplanetary magnetic field (IMF) and the occurrence of substorms. Dayside FACs respond promptly to changes in IMF B_Y, but the nightside response is delayed by up to an hour and can take up to 4 hr to develop fully, especially during northward IMF. Nightside FAC asymmetries grow during substorm growth phase when the IMF has a significant B_Y component, and also promptly at substorm onset. Our findings suggest that magnetotail twisting and/or B_Y penetration into the magnetotail, due to subsolar reconnection with east-west orientated IMF, are the main cause of these nightside FAC asymmetries and that asymmetries also arise due to magnetotail reconnection of these twisted field lines.

1. Introduction

Field-aligned currents (FACs), also known as Birkeland currents, are a fundamental component of magnetosphere-ionosphere coupling, which in turn is driven to a large extent by solar wind-magnetosphere coupling. Since 2010, the Active Magnetosphere and Planetary Electrodynamics Response Experiment (AMPERE) (Anderson et al., 2008, 2000, 2002; Waters et al., 2001) has provided measurements of FACs in the Northern and Southern Hemispheres at 10-min cadence, using magnetometer observations from the Iridium constellation of 66 satellites. This has resulted in a renewed focus on FACs and their response to solar wind-magnetosphere coupling (e.g., Anderson et al., 2014; Clausen et al., 2012; Clausen, Baker, et al., 2013; Clausen, Milan, et al., 2013; Coxon et al., 2016, 2014a, 2014b; Murphy et al., 2013; Wilder et al., 2013), as recently reviewed by Coxon et al. (2017).

One approach to the analysis of FAC observations from AMPERE has been the application of principal component analysis (PCA), which provides a means of decomposing the polar patterns of FACs into their dominant modes of variation (Cousins et al., 2015; Milan et al., 2015, 2017). For instance, Cousins et al. (2015) and Milan et al. (2015) demonstrated that the region 1 and region 2 current systems (R1/R2) first identified by Iijima and Potemra (1976a, 1978) are indeed the dominant component of the polar FACs and that the region 0 (R0) cusp current system (Iijima & Potemra, 1976b; Iijima et al., 1978) is the second most important component. These studies also confirmed that the magnitude of the R1/R2 current patterns is controlled by the strength of the Dungey cycle flow in the magnetosphere (Dungey, 1961), related to the sense of the IMF B_Z component, whereas the polarity of the R0 currents reflects the dawn-dusk orientation of the IMF, that is, its B_Y component (Iijima et al., 1978). Milan et al. (2015) also identified a pattern consistent with NBZ (northward IMF B_Z) FACs, associated with lobe reconnection. These applications of PCA, while useful, treat the polar FAC pattern as a whole, whereas it is expected that the dayside and nightside current systems are to some extent decoupled in their behavior. This suggests that PCA should be applied to dayside and nightside FACs separately to investigate this decoupling, and this is the aim of the current paper.

The expanding/contracting polar cap model (Cowley & Lockwood, 1992; Lockwood & Cowley, 1992; Milan, 2015) implies that the magnetosphere is independently driven by magnetic reconnection occurring at the dayside magnetopause and in the magnetotail neutral sheet. The former is directly controlled by conditions in the solar wind (Milan et al., 2012) and the latter by the conditions in the magnetotail and the occurrence of substorms (Milan et al., 2007). In other words, periods of polar cap expansion (substorm growth phase) precede periods of polar cap contraction (substorm expansion phase), with a delay of up to an hour leading to significant variations in the open magnetic flux content of the magnetosphere and the latitude of the auroral zones. These expansion and contraction phases should be accompanied by enhanced FACs on the dayside followed by enhanced FACs on the nightside (Milan, 2013), behavior that has been confirmed by Anderson et al. (2014), Coxon et al. (2014b), and Milan et al. (2017). Prompt responses of nightside convection and FACs to changes in dayside reconnection have also been reported, interpreted as the propagation time of pressure perturbations from the magnetopause to the neutral sheet through the lobes (e.g., Snekvik et al., 2017, and references therein).

In addition, it is anticipated that the dayside and nightside responses to changes in solar wind conditions are also decoupled to some extent. Considering the example of sudden changes in the dawn-dusk orientation of the IMF, ionospheric convection in the dayside polar cap and the associated currents (e.g., Svalgaard, 1973) are expected to respond promptly as the magnetic tension forces on newly reconnected field lines change from being directed eastward to westward or vice versa (e.g., Cowley et al., 1991). The nightside convection pattern and FACs are also expected to respond, but the causes of this response, and the time delay associated with this response, are still debated. As newly opened field lines connected to the IMF with one sense of B_Y or the other are added to the lobes, three interconnected effects are thought to occur. The field lines are added to the duskside or dawnside of the lobes due to their motion under the influence of the flow of the solar wind and east-west tension forces, which (a) changes the magnetic pressure distribution in the lobes (e.g., Cowley, 1981; Milan et al., 2017; Tenfjord et al., 2017) and (b) leads to a penetration of the IMF B_Y component into the lobes as these field lines sink toward the neutral sheet (e.g., Khurana et al., 1996). Although the phrase B_Y *penetration* is commonly used in the literature, *induced* B_Y is a more correct terminology, and we will use that here. Under northward IMF, IMF $B_Z > 0$, and ongoing lobe reconnection, the induced B_Y is thought to be exacerbated by (c) a twisting of the magnetotail (e.g., Cowley, 1981). The pressure distribution is thought to control east-west flow asymmetries in the nightside portion of the convection pattern on open field lines (e.g., Milan et al., 2017), whereas the induced field is expected to create flow asymmetries on newly closed field lines, that is, as reconnection occurs in the neutral sheet. Lobe field lines reconnecting in the magnetotail with an induced B_Y component should create closed magnetic field lines that are tilted out of meridian planes, which will subsequently straighten as they convect sunward, leading to asymmetrical flow patterns in the nightside portions of the northern and southern convection patterns; such flow asymmetries and associated auroral effects can be produced by tail reconnection occurring during periods of northward IMF (so-called TRINNI events; e.g., Fear & Milan, 2012; Grocott et al., 2003, 2004, 2005, 2008; Milan et al., 2005; Pitkänen et al., 2015), or during southward IMF associated with substorms (e.g., Grocott et al., 2010; Østgaard et al., 2005; Reistad et al., 2016).

The timescales of these responses and the regions of the magnetotail most affected are still unknown. Tenfjord et al. (2017) has asserted that B_Y induction in the inner magnetosphere is caused by pressure balance changes and is produced promptly (within tens of minutes) on both dayside and nightside. Fear and Milan (2012) found that the local time of the formation of transpolar arcs, closely correlated with the sense of nightside flow asymmetries associated with TRINNIs ($B_Z > 0$), is best correlated with the sense of IMF B_Y if a time lag of 4 hr is applied; a similar subsequent study by Kullen et al. (2015) found a delay of 1–2 hr. Rong et al. (2015) showed that B_Y induction in the magnetotail occurs on timescales of 1–2 hr, and Browett et al. (2017) went on to show that the timescale was 1–2 hr for IMF $B_Z < 0$ and 3–4 hr for $B_Z > 0$; these results suggest that the time delay is associated with the strength of Dungey cycle magnetic flux transport and the finite time taken for field lines to sink toward the neutral sheet. Pitkänen et al. (2016) presented a case study in which magnetotail twisting took place on timescales of 1–3 hr and that the delay was dependent on the distance downtail of the observations. Milan et al. (2010) and Reistad et al. (2016) suggested that asymmetries in the magnetotail develop over several hours but that B_Y-associated asymmetric auroras and flow in the ionosphere also become apparent once magnetotail reconnection (substorm or TRINNI) commences, and the delay with which this occurs following a southward turning of the IMF is uncertain. In this scenario, the time taken for the B_Y change to affect the nightside flow and FAC pattern is dependent on the propagation of the B_Y induction

from the magnetopause to the neutral sheet within the Dungey cycle convection (which could in principle take several substorm cycles) and the occurrence of magnetotail reconnection.

In this study we apply PCA independently to the dayside and nightside portions of the FAC distribution measured by AMPERE and determine the time delay of responses in the patterns to step changes in IMF orientation and the occurrence of substorms.

2. Methodology

We perform PCA on AMPERE observations of the Birkeland currents from the Northern and Southern Hemispheres for the period 2010 to 2016, to quantify the day/night and dawn/dusk asymmetries of the FACs as they respond to solar wind driving. We then perform superposed epoch analyses of these responses relative to sharp transitions in polarity of IMF B_Y and B_Z and the occurrence of substorms, to investigate the timescales of evolution of the system from one state to another. The methodology is described in the following sections.

2.1. PCA of FACs

The method of analysis is described in detail in Milan et al. (2015). AMPERE current density maps are available at a cadence of 2 mins, but only maps produced at 10-min cadence are completely independent, and it is these maps that we include in our analysis. Prior to analysis, each AMPERE current density map is scaled to be a consistent size: a circle is fitted to the boundary between the R1 and R2 current rings, and the map is transformed such that the circle is centered on the geomagnetic pole and has a latitude of 70° geomagnetic latitude. The transformed data are sampled onto a grid that has 24 local time bins and forty 1° latitudinal bins (960 cells). The radius of the original fitted circle, Λ, measured in degrees of latitude, will be used below as a proxy for the size of the polar cap. Maps in which the current densities are so weak that the R1/R2 system cannot be reliably detected are discarded. In the period 2010 to 2016, 277,507 maps from the Northern Hemisphere could be processed (84% of the available maps); in the Southern Hemisphere this number was 237,105 (72%).

In the original analysis of Milan et al. (2015), each such map was viewed as a vector, $\mathbf{J}$, in 960 dimensions, $\mathbb{R}^{960}$, with the data set as a whole representing a distribution of points in $\mathbb{R}^{960}$. Applied to this data, PCA determines 960 orthogonal directions (principal axes) that most efficiently describe the variance in the set of vectors, sorted into descending order of importance. These basis vectors can be viewed as patterns on the original grid, which we term eigenFACs. Any of the original maps that contributed to the analysis can be reconstructed as a linear combination of these eigenFACs (see below). The most significant eigenFACs that resulted from the original analysis by Milan et al. (2015) can be seen in Figure 2 of that paper.

In the present study, rather than performing the analysis on the full 960-cell grid, we first separate each $\mathbf{J}$ into dayside and nightside portions, $\mathbf{J}^D$ and $\mathbf{J}^N$, defined as 11 MLT sectors from 07 to 17 hr for the dayside and from 19 to 05 hr for the nightside. Only colatitudes between 5 and 40° are considered, to preclude a large number of closely spaced grid cells near the pole from dominating the analysis, hence $\mathbf{J}^D, \mathbf{J}^N \in \mathbb{R}^{440}$. PCA is then performed separately on the dayside and nightside portions of the grid, and separately in the Northern and Southern Hemispheres. The resulting eigenFACs from the dayside analysis are labeled $\mathbf{D}_i^{\mathrm{NH}}$ and $\mathbf{D}_i^{\mathrm{SH}}$, $i = 1, 2, 3, \ldots$, for the Northern and Southern Hemispheres, respectively, where $i = 1$ is the most significant eigenFAC. Similarly, the nightside eigenFACs are labeled $\mathbf{N}_i^{\mathrm{NH}}$ and $\mathbf{N}_i^{\mathrm{SH}}$.

The six most significant eigenFACs from each PCA analysis are presented in Figure 1. To the left, the dayside eigenFACs from the Northern and Southern Hemispheres are compared side-by-side, in descending order of significance down each column; to the right, the nightside eigenFACs are compared. Red and blue colors represent positive and negative values, respectively; these should not necessarily be interpreted as upward and downward currents, for reasons that will be explained below. The bottom panels present the percentage of the variance in the original dataset that is described by each eigenFAC.

$\mathbf{D}_1^{\mathrm{NH}}$ and $\mathbf{D}_1^{\mathrm{SH}}$ are consistent with the dayside portion of the R1/R2 system. The two patterns, despite being computed from two entirely independent data sets (the AMPERE technique treats the Northern and Southern Hemispheres separately) are very similar in nature. We quantify this similarity with the coefficient of correlation between elements of $\mathbf{D}_1^{\mathrm{NH}}$ and $\mathbf{D}_1^{\mathrm{SH}}$; in this case $r = 0.96$. The same is true for $\mathbf{N}_1^{\mathrm{NH}}$ and $\mathbf{N}_1^{\mathrm{SH}}$, the nightside R1/R2 system, except here $r = 0.99$. In fact, we find that $r > 0.89$ for all the eigenFAC pairs presented in Figure 1, with the exception of the $\mathbf{D}_4$ and $\mathbf{D}_5$ pairs (these two pairs seem to be mixed together by the analysis, an indication that the patterns are very similar in significance). The correlation is greater on the nightside than the dayside. Indeed, examining the next six eigenFACs on the nightside ($i = 7, \ldots, 12$, not shown), we find

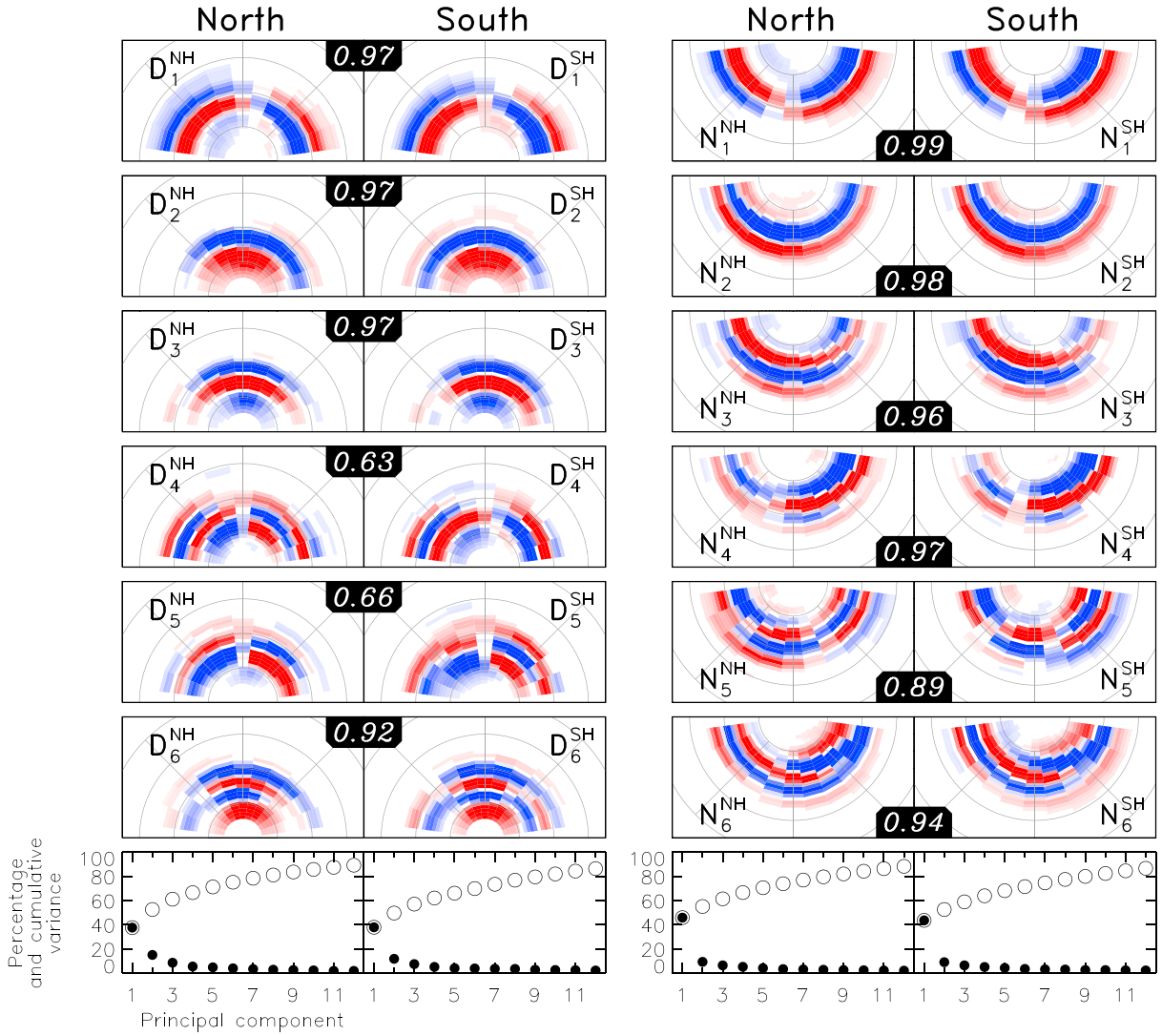

Figure 1. The first six eigenFACs for the dayside and nightside portions of the Northern and Southern Hemispheres Active Magnetosphere and Planetary Electrodynamics Response Experiment field-aligned current distributions, for the years 2010 to 2016. Each panel is presented in a magnetic local time and magnetic latitude frame, where magnetic latitudes are scaled such that the boundary between R1 and R2 FACs occurs at 70° (see text for details). Each north-south pair of eigenFACs has a coefficient of correlation quantifying their similarity. Bottom panels show the variance in the FACs explained by the first 12 eigenFACs. FAC = field-aligned current.

that although the value of r decreases with increasing i, similar features can be seen in each pair. That is, although the significance of eigenFACs decreases with increasing i, reproducible features exist in the eigenFACs determined independently from the Northern and Southern Hemispheres, to at least $i = 12$. This suggests that the patterns we have computed are robust modes of coherent variation in the terrestrial FAC systems. Due to the similarity between the NH and SH (Northern and Southern Hemispheres) eigenFACs, from this point onward we use the NH eigenFACs, henceforth $\mathbf{D}_i$ and $\mathbf{N}_i$, to characterize both NH and SH observations.

The eigenFACs that result from the PCA analysis are orthogonal, so any of the original FAC maps, for example, $\mathbf{J}^D$ or $\mathbf{J}^N$, can be represented as a linear combination of the eigenFACs. For instance, the dayside or nightside portion of a $\mathbf{J}$ can be expanded as

$$\mathbf{J}^D = \sum_{i=1}^{M} \alpha_i \mathbf{D}_i, \qquad \mathbf{J}^N = \sum_{i=1}^{M} \beta_i \mathbf{N}_i, \tag{1}$$

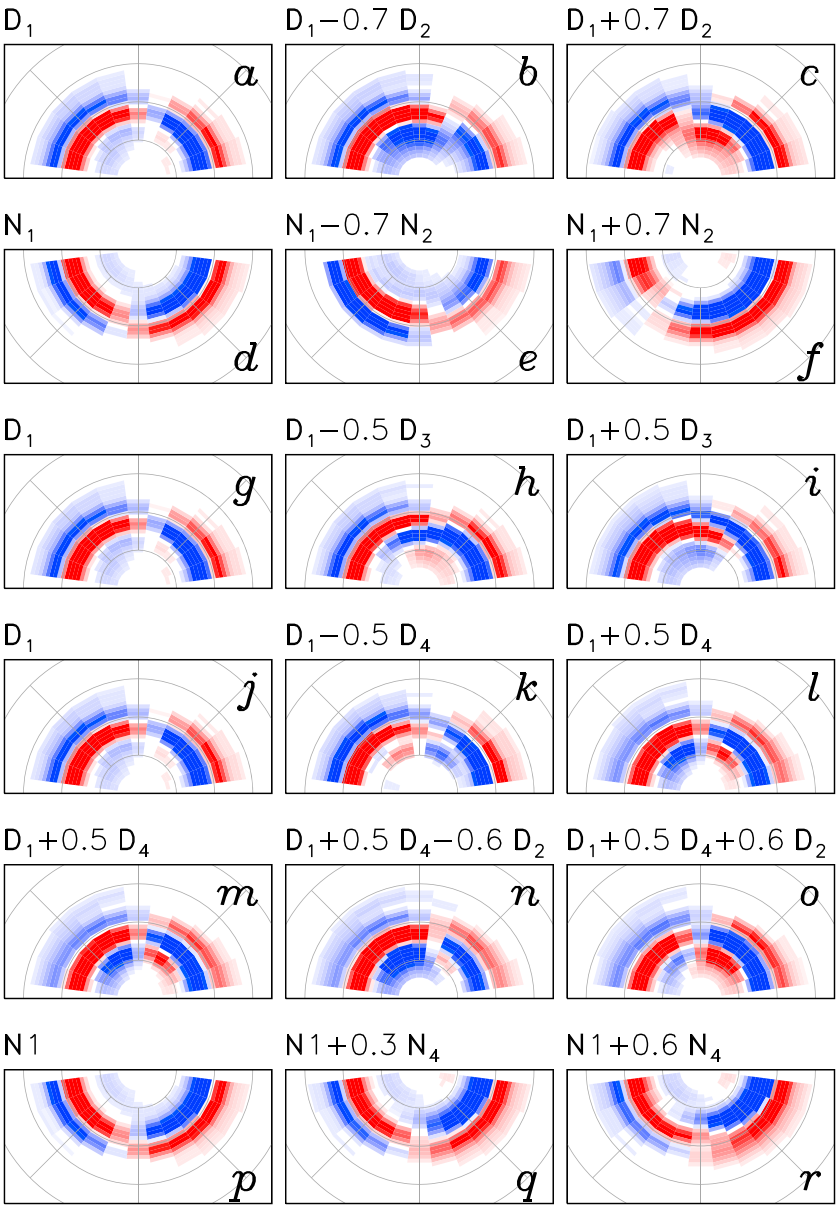

Figure 2. The effect of adding and subtracting different combinations of eigenFACs. All eigenFACs shown are for the Northern Hemisphere. Red and blue represent upward and downward FACs. See text for details. FACs = field-aligned currents.

where M is the number of available eigenFACs, $M = 440$. The α_is and β_is are coefficients that can be determined from the *overlap* between **J** and each eigenFAC:

$$\alpha_i = \mathbf{J}^D \cdot \mathbf{D}_i, \qquad \beta_i = \mathbf{J}^N \cdot \mathbf{N}_i, \tag{2}$$

where in principle α_i and β_i can be positive or negative. As these coefficients can be positive or negative, positive and negative values in the eigenFACs do not necessarily represent upward and downward FACs: however, once the sum of eigenFACs is considered (i.e., equation (1)), as will be explored in Figure 2, then positive and negative values represent upward and downward FACs, respectively, which we indicate by red and blue colors.

The rationale of PCA is that only the first few terms in equation (1) are significant, and a reasonable reconstruction of **J** can be achieved with a sum over m terms where $m \ll M$; that is, the current density maps can be decomposed into a small number of coefficients or principal components. Indeed, approximately 70–75%

of the variance in the original data set is explained by the first six eigenFACs (bottom panels of Figure 1) and if the first 12 eigenFACs are included this rises to close to 90%. In the PCA of Milan et al. (2015), close to 150 eigenFACs were needed to achieve this level of description, indicating that treating the dayside and nightside independently captures the behavior of the magnetosphere with greater fidelity.

EigenFACs $\mathbf{D}_1$ and $\mathbf{N}_1$ resemble the dayside and nightside portions of the R1/R2 FACs identified by Iijima and Potemra (1976a), which suggests that we can use the coefficients α_1 and β_1 computed from a given $\mathbf{J}$ to quantify the overall FAC magnitude associated with Dungey cycle convection. We expect these to be modulated by changes in IMF B_Z and the occurrence of substorms. Indeed, we expect that each coefficient quantifies a different aspect of the FAC response to magnetospheric behavior. Figure 2 illustrates the result of combining various eigenFACs, in a manner akin to equation (1). Panels a–c show the effect of adding $\mathbf{D}_2$ to $\mathbf{D}_1$, which is to shift the local time at which the R1 currents reverse polarity from upward to downward (the R2 currents are unaffected) and introducing an R0 current in the dayside polar cap. This is consistent with the expected patterns associated with dawnward or duskward orientated IMF so α_2 is expected to correlate with IMF B_Y, as demonstrated by Milan et al. (2015). Similarly, the combination of $\mathbf{N}_2$ with $\mathbf{N}_1$ (panels d–f) changes the local time of the reversal of the polarity of both R1 and R2 currents on the nightside and, as we will show below, β_2 captures IMF B_Y-associated asymmetries in the nightside FACs. Panels g–i indicate that $\mathbf{D}_3$ also introduces B_Y associated asymmetries into the dayside FACs. Panels j–l show that $\mathbf{D}_4$ produces R1/R2 sense FACs in the dayside polar cap when it is subtracted from $\mathbf{D}_1$ but produces FACs consistent with northward B_Z (NBZ) currents, associated with lobe reconnection and reverse lobe convection cells, when added. Panels m–o show the effect of adding $\mathbf{D}_2$ to the NBZ currents: to enlarge either the prenoon or postnoon NBZ FAC in a manner consistent with nonzero IMF B_Y. Finally, panels p–r show the effect of adding $\mathbf{N}_4$ to $\mathbf{N}_1$, which will be discussed later. We note that none of the eigenFACs represent changes in the latitude of the current ovals, as this behavior has been removed by our preprocessing.

2.2. Superposed Epoch Analyses

From each 2-min AMPERE map $\mathbf{J}$ collected over the period 2010 to 2016, we compute the coefficients α_i and β_i, which quantify the contributions made by each eigenFAC to the overall FAC pattern. We then perform superposed epoch analyses of these coefficients relative to (a) sharp transitions in the polarity of IMF B_Y and B_Z and (b) the occurrence of substorms.

IMF components in Geocentric Solar Magnetic (GSM) coordinates were extracted from the 1-min OMNI database (King & Papitashvili, 2005). A time t_0 is designated as a $B_Z(+/-)$ transition when 80% of points are $B_Z > 2$ nT in the 20 min prior to t_0 and 80% of points are $B_Z < -2$ nT in the following 80 min. $(-/+)$ transitions are found in a similar manner. A total of 193 $(+/-)$ and 162 $(-/+)$ transitions were identified. A time t_0 is designated a $B_Y(+/-)$ transition if 80% of points are $B_Y > 2$ nT in the previous 20 min, and 80% of points are $B_Y < -2$ nT in the following 40 min. These transitions are then classified as occurring under northward or southward IMF conditions if the mean value of B_Z over the hour considered is $\bar{B}_Z > 3$ or $\bar{B}_Z < -3$ nT; all other transitions are discarded. A similar analysis identifies $B_Y(-/+)$ transitions. A total of 86 and 93 northward and southward IMF B_Y transitions were found.

We employ the Newell and Gjerloev (2011) substorm onset list derived from SuperMAG observations, which contains 9,294 onsets during the period 2010 to 2016. In addition to using this full list, we identify substorms that occur during ongoing IMF $B_Y < 0$ conditions and $B_Y > 0$ conditions. The criteria we apply in each case is that $|B_Y| > 4$ nT for 80% of the time in the 4 hr centered on substorm onset. Eight hundred seventy-eight substorms meet these criteria.

Figures 3–6 show superposed epoch analyses of several parameters with respect to transitions in IMF B_Z (Figure 3), substorms (Figures 4 and 6), and transitions of B_Y (Figure 5), from $t_0 - 2$ to $t_0 + 4$ hours in each case. The standard error on the mean is represented by the gray region in each panel (in some cases this is no thicker than the black line).

Our results indicate that NH and SH responses are almost identical, so we aggregate observations from both hemispheres in these analyses. As discussed above, some eigenFACs represent current systems that are controlled by the dawn-dusk component of the IMF, such that their coefficients α_i and β_i are expected to be correlated with IMF B_Y. In such cases, if the correlation is positive in the NH, it is negative in the SH and vice versa. In addition, the response is mirrored for $(+/-)$ and $(-/+)B_Y$ transitions. In these cases we have combined NH and SH observations during both polarities of transition, by reversing the sign of the coefficients

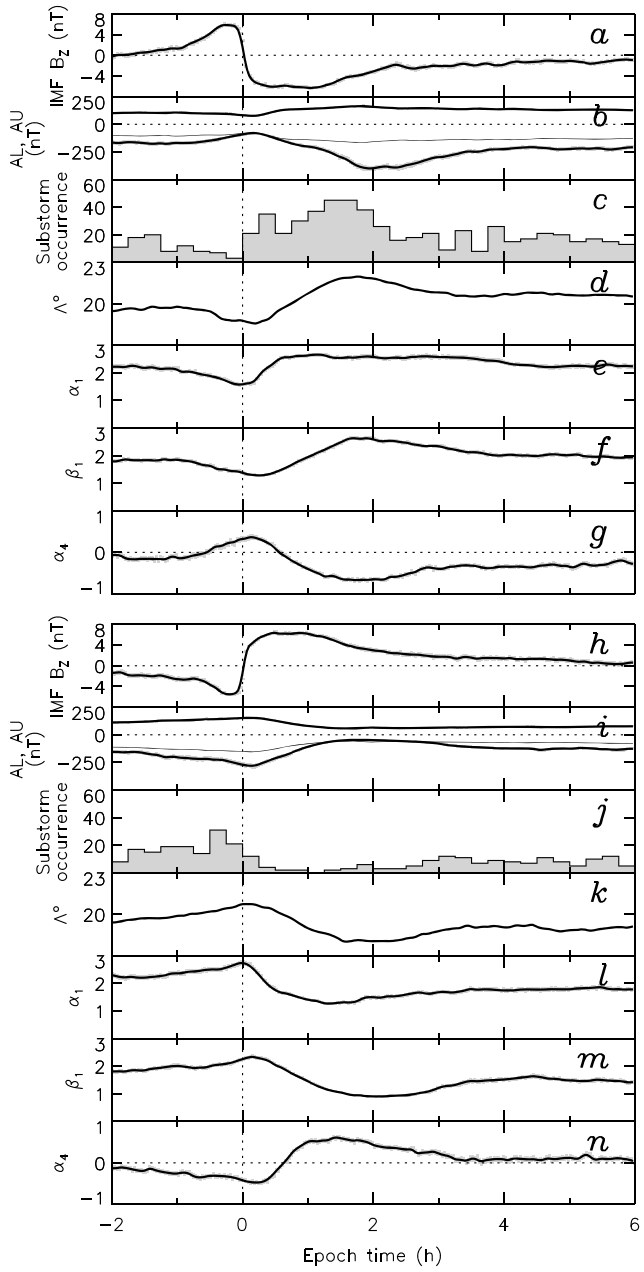

Figure 3. Superposed epoch analysis of FAC responses to reversals of the north-south component of the IMF. Panels a–g present north-south reversals, and panels h–n the south-north reversals. (a, h) IMF B_Z, (b, i) AU and AL electrojet indices (thin line is −AU), (c, j) substorm occurrence in 15-min bins, (d, k) the radius of the R1/R2 current oval, (e–g, l–n) principal component analysis coefficients α_1 and β_1 (dayside and nightside R1/R2 FAC magnitudes), and α_4 (dayside NBZ current magnitude). FACs = field-aligned currents; IMF = interplanetary magnetic field.

such that the changes are consistent with a (+/−) transition in the Northern Hemisphere; where this has been done, we indicate the parameter with an asterisk, for example, B_Y^*, α_2^* (see Figures 5 and 6).

3. Observations and Discussion

Figure 3 presents a superposed epoch analysis of (+/−) transitions in B_Z: (a) B_Z, (b) AU and AL, (c) substorm occurrence in 15-min bins, (d) radius of the current ovals, Λ, the (e) dayside, and (f) nightside R1/R2 current magnitude, α_1 and β_1, respectively, and (g) α_4. In panel (b), in addition to AU and AL, we include −AU to indicate when substorm activity is going on, that is, when AL < −AU. Panels (h)–(n) show a similar analysis for the (−/+)B_Z transitions.

We first discuss the (+/−) transitions. On average, B_Z rises to 6 nT shortly before the transition and then averages −6 nT from t_0 + 10 to t_0 + 70 min after the transition, before gradually decreasing in magnitude over the following 4 hr. AU and AL show minor activity at the start of the analysis, 120 and −190 nT, reducing to ±100 nT as B_Z becomes increasingly positive prior to t_0. Following the southward turning, AU and AL increase in magnitude, AU rising to 160 nT and AL falling to −420 nT at t_0 + 120 min. These gradually decline in magnitude thereafter as the magnitude of B_Z decreases. The AU/AL behavior is reflected in the substorm occurrence, which falls as B_Z becomes increasingly positive and then ramps up until t_0 + 90 min, before falling again. The radius of the current ovals decreases slightly prior to t_0 when B_Z is positive. Then, from t_0 + 10 to t_0 + 110 min, the radius increases, before gradually declining again. During this 100-min interval, the opening of flux at the dayside dominates the closure of flux on the nightside and the polar cap expands. As the polar cap expands, substorm onset becomes more likely, and after t_0 + 90-min nightside reconnection dominates such that the polar cap contracts on average.

The dayside R1/R2 magnitude, α_1, falls gradually prior to t_0 and then begins to rise at t_0 + 10 min before plateauing at t_0 + 35 min. We interpret the 10-min delay between t_0 and the rise in α_1 as the propagation delay from the arrival of the IMF at the bow shock and the communication of changes in dayside reconnection at the magnetopause to the ionosphere. It thereafter takes 25 min for the changes in convection to fully develop (cf. (Khan & Cowley, 1999). The nightside FAC magnitude, β_1, also falls prior to t_0 and for the following 15 min, before rising over a period of 90 min before gradually diminishing; this variation closely mirrors the behavior of AL. The onset of the nightside response is almost as prompt as the dayside (the short delay is interpreted by Snekvik et al. (2017) as the time taken for pressure perturbations to propagate through the lobes) but takes the onset of substorm activity and associated nightside reconnection for the response to maximize. As indicted in Figures 2j–2l, $\alpha_4 > 0$ is indicative of NBZ FACs associated with reverse lobe cells, and this situation develops in the lead up to t_0; it then takes until t_0 + 30 min for this signature to reverse.

In the case of (−/+) transitions, the occurrence of substorm onsets is roughly uniform as t_0 approaches but decreases dramatically following the northward turning: we see no evidence of substorm onsets triggered by the northward turnings, as has been proposed and refuted by previous workers (e.g., Wild et al., 2009, and references therein). Substorm activity as measured by AU/AL increases slowly toward t_0 + 5 min, but thereafter decreases to reach a minimum by t_0 + 70 min. That is, although substorm onsets cease after the northward turning, residual substorm activity associated with substorms that commenced prior to the turning persists for up to an hour. The radius of the oval decreases over the period t_0 + 10 to t_0 + 100 min,

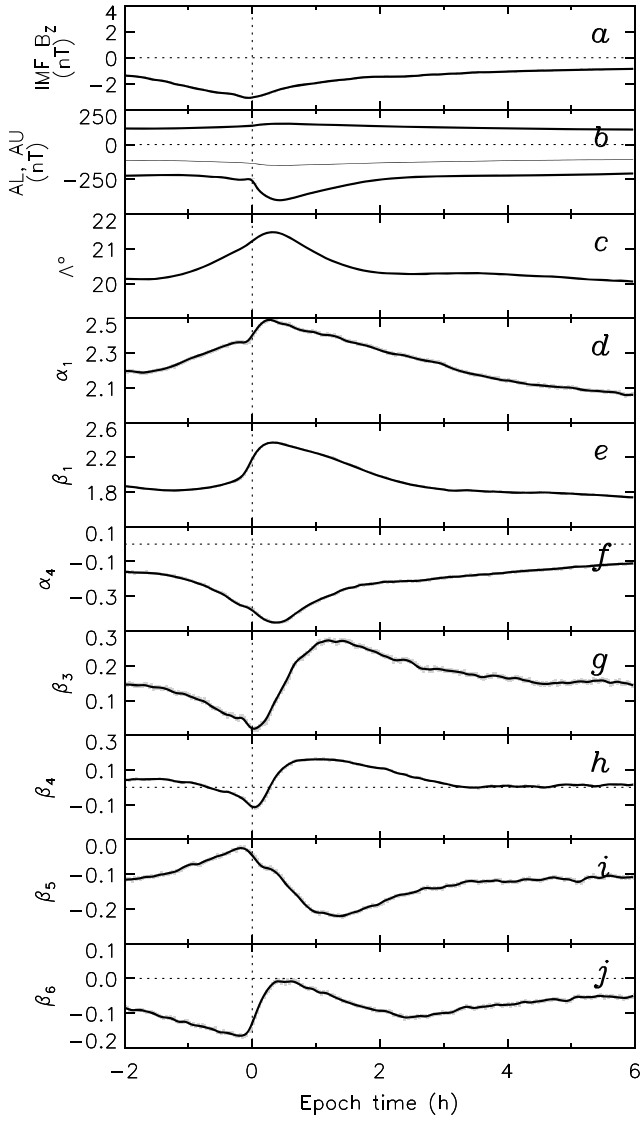

Figure 4. Superposed epoch analysis of FAC responses to substorm onset. (a) IMF B_Z, (b) AU and AL electrojet indices (thin line is −AU), (c) the radius of the R1/R2 current oval, (d–j) principal component analysis coefficients α_1 and β_1 (dayside and nightside R1/R2 FAC magnitudes), and α_4 (dayside NBZ current magnitude), β_3 to β_6 (other substorm-associated current systems). FACs = field-aligned currents; IMF = interplanetary magnetic field.

associated with residual nightside reconnection associated with this ongoing substorm activity following the northward turning. However, α_1 increases gradually while $B_Z > 0$ prior to t_0 but decreases sharply between $t_0 + 5$ and $t_0 + 60$ min. While the onset of the dayside R1/R2 decrease is prompt, we interpret the length of time over which the decrease occurs as the continued influence of ongoing nightside reconnection on the dayside convection pattern. The nightside response does not begin until $t_0 + 10$ min, and β_1 does not reach a minimum until $t_0 + 120$ min, which we again interpret as ongoing nightside reconnection. α_4 is negative prior to the turning and does not become positive until $t_0 + 45$, maximizing at $t_0 + 80$ min: apparently, it takes some time for reverse lobe cells to fully develop following a northward turning, as previously noted by Grocott and Milan (2014).

Figure 4 presents a superposed epoch analysis of 9,294 substorm onsets: (a) B_Z, (b) AU and AL, (c) radius of the current ovals, Λ, the (d) dayside, and (e) nightside R1/R2 current magnitude, α_1 and β_1, respectively, and a number of other dayside and nightside coefficients. The behavior of B_Z, AL, AU, and Λ are, as has been reported many times previously (e.g., Coxon et al., 2014b), as follows: B_Z becomes increasingly negative prior to t_0 and becomes less negative after; AL and AU increase in magnitude up to t_0, AL shows the onset of a substorm bay at t_0, and then activity gradually quietens; and the oval radius grows prior to t_0 and then decreases after $t_0 + 15$ min over the next 2 hr, as expected for substorm growth (polar cap expansion) and onset and recovery (polar cap contraction).

The dayside R1/R2 FACs (α_1) increase during the growth phase and then step up following substorm onset, maximizing at $t_0 + 15$ min, before gradually declining. The nightside R1/R2 FACs (β_1) show little variation during the growth phase but ramp up at onset, peaking at $t_0 + 10$ min, before declining to preonset levels by $t_0 + 120$ min. These variations suggest that the strength of dayside convection increases during the growth phase due to dayside reconnection, with an enhancement during the expansion phase due to nightside reconnection, which is consistent with the expanding/contracting polar cap model (Cowley & Lockwood, 1992; Lockwood & Cowley, 1992; Milan, 2015). On average, the substorm growth phase lasts 90 min, and the combined expansion and recovery phase lasts 120 min.

For completeness we also show the variations of other dayside and nightside FAC patterns. The dayside coefficient α_4 (NBZ-like FACs) is negative throughout but is most negative at $t_0 + 15$ min, largely mirroring the variation in IMF B_Z, with a slight delay, as described above. The other nightside coefficients shown, β_3 to β_6, each show well-defined variations associated with substorm growth, onset, and recovery phase, with a variety of timescales of response before and after onset. This indicates that the corresponding FAC patterns are associated with substorm processes and that the overall nightside FAC pattern evolves as substorms develop. A detailed description of these variations is outside the scope of the present paper and is reserved for a follow-on study.

Figure 5 shows the response of FAC coefficients α_2^*, α_3^*, and β_2^* to transitions in IMF B_Y during periods of $\bar{B}_Z < -3$ nT (upper panels) and $\bar{B}_Z > 3$ nT (lower panels). For both positive and negative B_Z, clear reversals in B_Y^* are observed from +7 to −7 nT over the period $t_0 - 10$ to $t_0 + 10$ min, with B_Z remaining positive or negative for the majority of the 8-hr duration of the figure.

We consider the $B_Z < 0$ case first. All three coefficients show a clear transition associated with the reversal of B_Y^*. The dayside coefficient α_2^* transitions over the period t_0 to $t_0 + 30$ min, with the reversal occurring at $t_0 + 18$ min; α_3^* transitions over the period t_0 and $t_0 + 20$ min, with the reversal occurring at $t_0 + 10$ min. We interpret $\mathbf{D}_3$ as a transitionary phase, which occurs as B_Y reverses, whereas $\mathbf{D}_2$ represents the fully formed R0

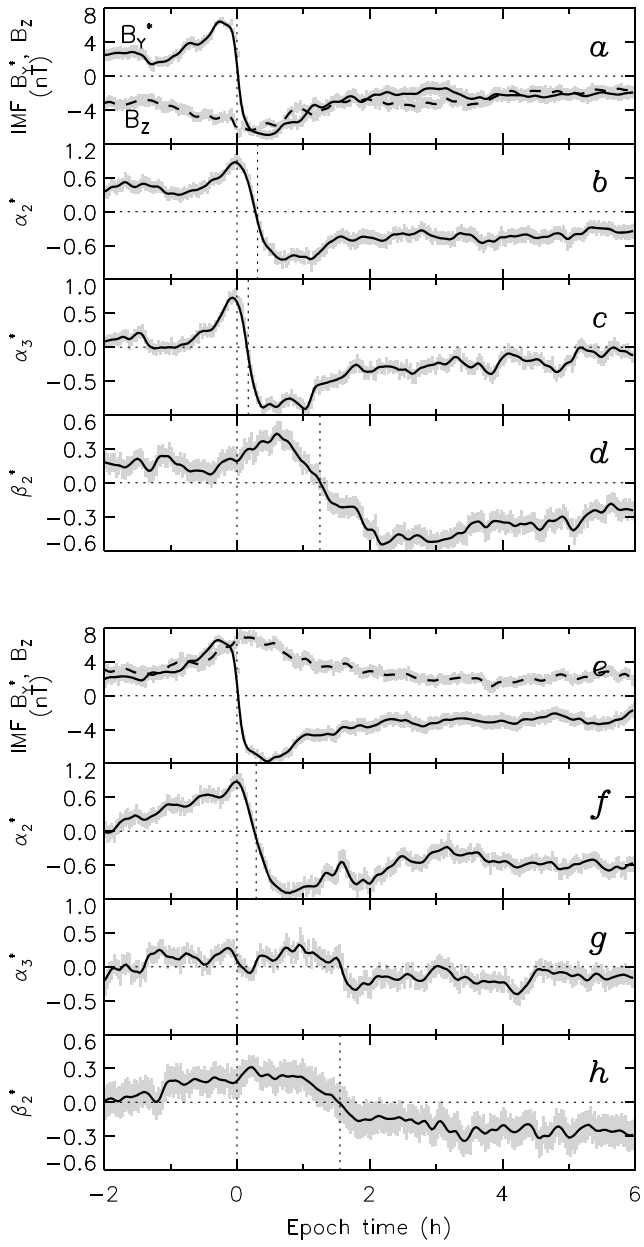

Figure 5. Superposed epoch analysis of FAC responses to reversals of the dawn-dusk component of the IMF. Panels a–d present reversals during ongoing southward IMF, and panels e–h during northward IMF. (a, e) IMF B_Y^* and B_Z, (b–d, f–h) principal component analysis coefficients α_2^* and α_3^* (both related to dayside R0 FACs), and β_2^* (nightside B_Y-associated FAC asymmetry). FACs = field-aligned currents; IMF = interplanetary magnetic field.

FAC system. The nightside transition in β_2^* is delayed: the transition occurs between $t_0 + 40$ and $t_0 + 120$ min, with the reversal at $t_0 + 75$ min.

In the case of $B_Z > 0$, both α_2^* and β_2^* show clear transitions. The variation of α_3^* is unclear, and we do not assign a timescale to the reversal. The magnitude and timescale of the α_2 transition is similar to the $B_Z < 0$ case. The β_2 transition begins later at $t_0 + 60$ min, and the reversal occurs near $t_0 + 95$ min; the magnitude of β_2^* is less in this case, and the error on the mean is larger, suggesting that nightside FACs are weaker during northward IMF and changes related to B_Y are less reproducible. Strong nightside east-west flows associated with B_Y are known to occur during northward IMF (TRINNIs; Fear & Milan, 2012; Grocott et al., 2004, 2003, 2008, 2005; Milan et al., 2005), but the nightside conductance is expected to be low at such times (Milan et al., 2005), so any associated FACs will be weak.

It is interesting that the variation of α_2^* is as clear for $B_Z > 0$ as $B_Z < 0$. This indicates that although lobe reconnection is occurring in the former case, rather than subsolar magnetopause reconnection, the tension forces and associated R0 current produced by nonzero B_Y are as significant, and changes in polarity occur as promptly as in the $B_Z < 0$ case. The effect of $\mathbf{D}_4$ on NBZ currents is illustrated in Figures 2m and 2n, which shows that it causes either the prenoon or postnoon NBZ FAC to enlarge depending on the sign of B_Y. α_3^* responds very promptly to changes in B_Y when $B_Z < 0$ but does not have a clear signature for $B_Z > 0$, indicating that this feature is associated with subsolar reconnection only.

The B_Y-associated changes on the nightside are significantly delayed with respect to the arrival of the transition in the IMF. The beginning of the response is later in the $B_Z > 0$ case, 60 min rather than 40, and the reversal takes longer. These statistics are for the case where $|\bar{B}_Z| > 3$ nT. We have undertaken similar studies in which we stipulate that $|\bar{B}_Z|$ must be larger, to more strongly differentiate between northward and southward IMF cases, though this leads to a reduction in the number of B_Y transitions that match our selection criteria. However, it is clear from these studies that as the IMF becomes more strongly southward the nightside reversal occurs faster (closer to $t_0 + 60$ min) and for strongly northward IMF the reversal is even further delayed. These timescales are consistent with the findings of Fear and Milan (2012), Rong et al. (2015), and Browett et al. (2017), which are thought to be associated with induction of B_Y into the magnetotail lobes, with a delay associated with the strength of the convection cycle. We do not see a nightside timescale of a few tens of minutes, as reported by Tenfjord et al. (2017) in the inner magnetosphere, suggesting that the B_Y asymmetries in the inner magnetosphere are not significant for magnetosphere-ionosphere coupling or do not immediately manifest themselves as changes in convection and FACs.

In Figure 6, we perform a superposed epoch analysis of substorms occurring during ongoing $B_Y < 0$ and $B_Y > 0$ conditions. Panel (a) shows that $B_Y^* \approx 8$ nT in the 4 hr centered on onset, indicating that the two classes of substorm are well separated. Panels (a)–(d) also show the variations of B_Z, AU and AL, radius Λ, and R1/R2 FAC magnitudes α_1 and β_1. All these show similar variations to the full substorm list presented in Figure 4, so the B_Y component does not significantly affect these aspects of the FAC response to substorm onset.

Panels (e) and (f) present the dayside and nightside responses α_2^* and β_2^* to B_Y^*. The dayside R0 current varies linearly with B_Y^*, responding promptly to changes in B_Y^*. However, the nightside FAC asymmetry grows throughout the substorm growth phase, before plateauing and decreasing after onset. This indicates that the asymmetry grows as subsolar reconnection with a given sense of B_Y continues and as this newly opened flux is convected into the magnetotail lobes, consistent with the induction of B_Y into the magnetotail.

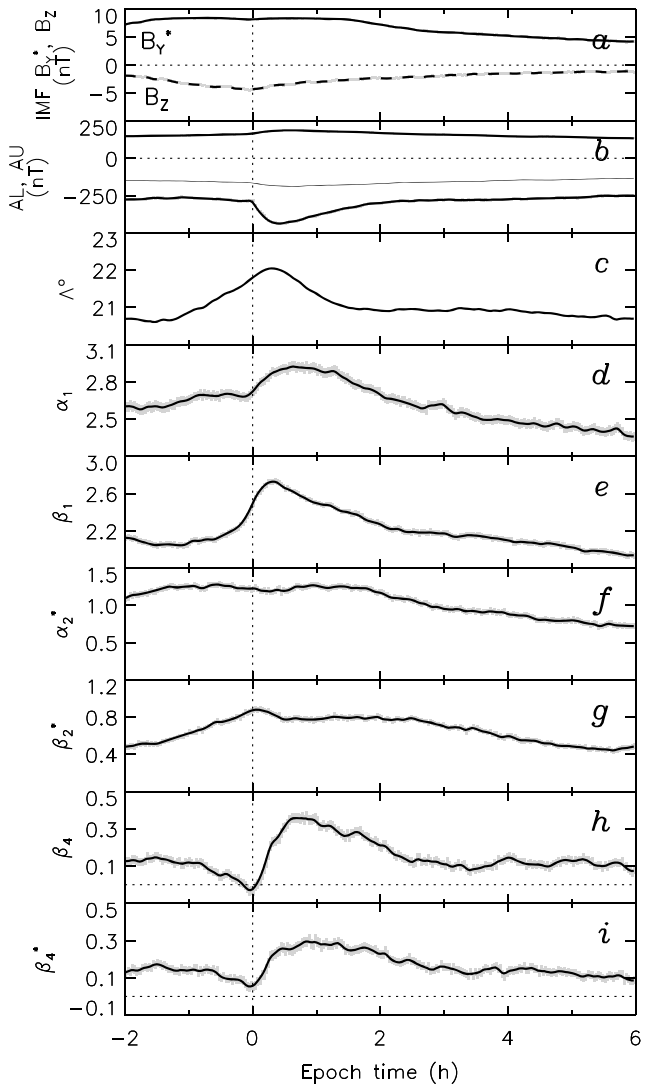

Figure 6. Superposed epoch analysis of FAC responses to substorm onset during substorms occurring during periods with a significant IMF B_Y component. (a) IMF B_Y^* and B_Z, (b) AU and AL electrojet indices (thin line is −AU), (c) the radius of the R1/R2 current oval, (d–i) principal component analysis coefficients α_1 and β_1 (dayside and nightside R1/R2 FAC magnitudes), α_2^* and β_2^* (dayside and nightside B_Y-associated FAC asymmetries), and β_4 and β_4^* (another substorm-associated current system). FACs = field-aligned currents; IMF = interplanetary magnetic field.

Panels (h) and (i) present the response of eigenFAC $\mathbf{N}_4$ to substorm onset, quantified as β_4 and β_4^*. β_4 represents the overall response of $\mathbf{N}_4$ in both NH and SH, that is, β_4^{NH} and β_4^{SH}, whereas β_4^* is the combination of β_4^{NH} and $-\beta_4^{SH}$. If $\mathbf{N}_4$ was controlled entirely by B_Y such that β_4^{NH} and β_4^{SH} responded oppositely to each other, then we would expect β_4 to average to 0. If, on the other hand, $\mathbf{N}_4$ had no dependence on B_Y, we would expect β_4^* to average to 0. That both β_4 and β_4^* respond positively following substorm onset suggests that $\mathbf{N}_4$ is added to the FAC pattern during substorms but that its magnitude is dependent on the orientation of B_Y during the growth phase of the substorm. Figures 2p–2r illustrate the effect of adding $\mathbf{N}_4$ to $\mathbf{N}_1$, which is to progressively thin the R1/R2 currents in the premidnight sector, thicken the currents in the postmidnight sector, and cause an overlap of the upward and downward R1 currents at midnight, with downward current poleward of the upward current. The sense of this current overlap appears to agree with the B_Y distortion of the postonset convection pattern reported by Grocott et al. (2010) (see their Figure 4d and compare the relatively east-west symmetrical pattern of flows out of the polar cap in the NH, $B_Y < 0$ and SH, $B_Y > 0$ cases, with the westward kink in the midnight sector flows out of the polar cap in the other cases). Our results show that this flow asymmetry grows promptly following substorm onset, maximizing by t_0+20 min. This suggests that in addition to the progressive increase in induced B_Y observed during the growth phase, asymmetries associated with B_Y also appear at substorm onset, suggesting that these are produced by reconnection of the twisted field lines.

4. Conclusions

We have presented a PCA of Birkeland current measurements from the AMPERE experiment, focusing on changes in the currents associated with reversals of the orientation of the IMF in both the north-south and east-west directions, and on substorm onset. The main conclusions are as follows:

EigenFACs are computed independently for the dayside and nightside FACs. Approximately 90% of the variance in the original data set is captured in the first 12 eigenFACs on both the dayside and nightside. This is significantly higher than when the whole polar region is treated together (Milan et al., 2015), indicating that variations in the FACs on the dayside and nightside are decoupled. EigenFACs computed independently in the Northern and Southern Hemispheres are very similar, showing that these are robust estimates of the main modes of variability of the FACs.

In response to southward turnings of the IMF, the dayside R1/R2 FACs increase with a delay of 10 min, and maximize after 30 min. The nightside R1/R2 FACs take 90 min to maximize, consistent with the time taken for substorm expansion to follow the onset of the growth phase.

After northward turnings, dayside R1/R2 FACs decrease over a period of 60 min, the timescale for ongoing substorm activity to subside. The nightside R1/R2 FACs also decrease but over a period that suggests that residual magnetotail reconnection, associated with a reduction in the size of the polar cap, continues following the cessation of dayside subsolar reconnection. NBZ FACs appear to take between 45 and 90 min to fully develop following the northward turning.

Both dayside and nightside FACs respond to changes in the east-west component of the IMF. These changes begin promptly on the dayside but take up to 45 min to fully develop. The nightside response is delayed, by 40 min during southward IMF conditions and up to an hour during northward IMF. The change is not fully developed until 2 hr after the turning, the change being slower and weaker for periods of northward rather than southward IMF.

R1/R2 FACs on the dayside increase in magnitude during substorm growth phase and then peak 10 min after substorm onset; the nightside R1/R2 FACs do not show a significant increase during growth phase but also peak 10 min after onset. Several nightside eigenFACs show prompt responses at onset, indicating that the nightside FACs evolve in a complicated and rapidly varying manner during the expansion and recovery phases. Substorms occurring during periods when the IMF has a significant east-west component have a nightside FAC asymmetry that increases throughout the growth phase, but plateaus at substorm onset. On the other hand, nightside FAC asymmetries develop promptly at onset and manifest themselves over a period of 10 min.

Our findings support previous reports that nightside and magnetotail phenomena respond to changes in B_Y component of the IMF over a period of 2 hr during southward IMF and longer during northward IMF (e.g., Browett et al., 2017; Fear & Milan, 2012; Rong et al., 2015). Our findings also suggest that substorms play a significant role in the development of nightside FAC asymmetries: asymmetry grows during the growth phase, but asymmetries also develop promptly at onset (e.g., Milan et al., 2010; Reistad et al., 2016). These findings suggest that magnetotail twisting and/or IMF B_Y induction grow with ongoing dayside reconnection when the IMF has a significant B_Y component and that magnetotail reconnection of these field lines manifests asymmetries also. The timescale of the Dungey and substorm cycle, controlled by the north-south component of the IMF, modulates the development of the asymmetries. We do not find a nightside asymmetry with a timescale of tens of minutes following B_Y reversals, as reported by Tenfjord et al. (2017) in the inner magnetosphere and conclude that B_Y induction at geosynchronous orbit does not contribute significantly to magnetosphere-ionosphere coupling or that this effect is delayed until substorm onset.

Acknowledgments
S. E. M. and J. A. C. were supported by the Science and Technology Facilities Council (STFC), UK, grant ST/N000749/1; H. S. was supported by a STFC studentship. The work at the Birkeland Centre for Space Centre, University of Bergen, Norway, was supported by the Research Council of Norway/CoE under contract 223252/F50. We thank the AMPERE team and the AMPERE Science Center for providing the Iridium-derived data products; AMPERE products are available at http://ampere.jhuapl.edu. The OMNI data, including solar wind parameters and geomagnetic indices, were obtained from the GSFC/SPDF OMNIWeb interface at http://omniweb.gsfc.nasa.gov. The SuperMAG substorm list was downloaded from http://supermag.jhuapl.edu. For the ground magnetometer data from which this list was derived, we gratefully acknowledge the following: Intermagnet; USGS, Jeffrey J. Love; CARISMA, PI Ian Mann; CANMOS; The S-RAMP Database, PI K. Yumoto and K. Shiokawa; The SPIDR database; AARI, PI Oleg Troshichev; The MACCS program, PI M. Engebretson, Geomagnetism Unit of the Geological Survey of Canada; GIMA; MEASURE, UCLA IGPP and Florida Institute of Technology; SAMBA, PI Eftyhia Zesta; 210 Chain, PI K. Yumoto; SAMNET, PI Farideh Honary; the institutes who maintain the IMAGE magnetometer array, PI Eija Tanskanen; PENGUIN; AUTUMN, PI Martin Connors; DTU Space, PI Juergen Matzka; South Pole and McMurdo Magnetometer, PIs Louis J. Lanzarotti and Alan T. Weatherwax; ICESTAR; RAPIDMAG; PENGUIn; British Artarctic Survey; McMac, PI Peter Chi; BGS, PI Susan Macmillan; Pushkov Institute of Terrestrial Magnetism, Ionosphere and Radio Wave Propagation (IZMIRAN); GFZ, PI Juergen Matzka; MFGI, PI B. Heilig; IGFPAS, PI J. Reda; University of L'Aquila, PI M. Vellante; SuperMAG, PI Jesper W. Gjerloev.

References

Anderson, B. J., Korth, H., Waters, C. L., Green, D. L., Merkin, V. G., Barnes, R. J., & Dyrud, L. P. (2014). Development of large-scale Birkeland currents determined from the Active Magnetosphere and Planetary Electrodynamics Response Experiment. *Geophysical Research Letters*, *41*, 3017–3025. https://doi.org/10.1002/2014GL059941

Anderson, B. J, Korth, H., Waters, C. L., Green, D. L., & Stauning, P. (2008). Statistical Birkeland current distributions from magnetic field observations by the iridium constellation. *Annales Geophysicae*, *26*, 671–687. https://doi.org/10.5194/angeo-26-671-2008

Anderson, B. J., Takahashi, K., Kamei, T., Waters, C. L., & Toth, B. A. (2002). Birkeland current system key parameters derived from iridium observations: Method and initial validation results. *Journal of Geophysical Research*, *107*, 1079. https://doi.org/10.1029/2001JA000080

Anderson, B. J., Takahashi, K., & Toth, B. A. (2000). Sensing global Birkeland currents with iridium engineering magnetometer data. *Geophysical Research Letters*, *27*, 4045–4048. https://doi.org/10.1029/2000GL000094

Browett, S. D., Fear, R. C., Grocott, A., & Milan, S. E. (2017). Timescales for the penetration of IMF by into the Earth's magnetotail. *Journal of Geophysical Research: Space Physics*, *122*, 579–593. https://doi.org/10.1002/2016JA023198

Clausen, L. B. N., Baker, J. B. H., Ruohoniemi, J. M., Milan, S. E., & Anderson, B. J. (2012). Dynamics of the region 1 Birkeland current oval derived from the Active Magnetosphere and Planetary Electrodynamics Response Experiment (AMPERE). *Journal of Geophysical Research*, *117*, A06233. https://doi.org/10.1029/2012JA017666

Clausen, L. B. N., Baker, J. B. H., Ruohoniemi, J. M., Milan, S. E., Coxon, J. C., Wing, S., et al. (2013). Temporal and spatial dynamics of the region 1 and 2 Birkeland currents during substorms. *Journal of Geophysical Research: Space Physics*, *118*, 3007–3016. https://doi.org/10.1002/jgra.50288

Clausen, L. B. N., Milan, S. E., Baker, J. B. H., Ruohoniemi, J. M., Glassmeier, K.-H., Coxon, J. C., & Anderson, B. J. (2013). On the influence of open magnetic flux on substorm intensity: Ground- and space-based observations. *Journal of Geophysical Research: Space Physics*, *118*, 2958–2969. https://doi.org/10.1002/jgra.50308

Cousins, E. D. P., Matsuo, T., Richmond, A. D., & Anderson, B. J. (2015). Dominant modes of variability in large-scale Birkeland currents. *Journal of Geophysical Research: Space Physics*, *120*, 6722–6735. https://doi.org/10.1002/2014JA020462

Cowley, S. W. H. (1981). Magnetospheric asymmetries associated with the *y*-component of the IMF. *Planetary and Space Science*, *29*, 79–96.

Cowley, S. W. H., & Lockwood, M. (1992). Excitation and decay of solar wind-driven flows in the magnetosphere-ionosphere system. *Annales Geophysicae*, *10*, 103–115.

Cowley, S. W. H., Morelli, J. P., & Lockwood, M. (1991). Dependence of convective flows and particle precipitation in the high-latitude dayside ionosphere on the *x* and *y* components of the interplanetary magnetic field. *Journal of Geophysical Research*, *96*, 5557–5564.

Coxon, J. C., Milan, S. E., Carter, J. A., Clausen, L. B. N., Anderson, B. J., & Korth, H. (2016). Seasonal and diurnal variations in AMPERE observations of the Birkeland currents compared to modelled results. *Journal of Geophysical Research: Space Physics*, *121*, 4027–4040. https://doi.org/10.1002/2015JA022050

Coxon, J. C., Milan, S. E., Clausen, L. B. N., Anderson, B. J., & Korth, H. (2014a). The magnitudes of the Birkeland currents observed by AMPERE and their role in solar wind-magnetosphere-ionosphere coupling. *Journal of Geophysical Research: Space Physics*, *119*, 9804–9815. https://doi.org/10.1002/2014JA020138

Coxon, J. C., Milan, S. E., Clausen, L. B. N., Anderson, B. J., & Korth, H. (2014b). A superposed epoch analysis of the region 1 and region 2 Birkeland currents observed by AMPERE during substorms. *Journal of Geophysical Research: Space Physics*, *119*, 9834–9846. https://doi.org/10.1002/2014JA020500

Coxon, J. C., Milan, S. E., Korth, H., & Anderson, B. J. (2017). Ampère's law: A review of Birkeland current research using the iridium constellation. In A. Keiling, O. Marghitu, & M. Wheatland (Eds.), *Electric Currents in Geospace and Beyond, AGU Geophysical Monograph* (Vol. 235, pp. 568). Washington, DC: Wiley and Sons.

Dungey, J. W. (1961). Interplanetary magnetic fields and the auroral zones. *Physical Review Letters*, *6*, 47–48.

Fear, R. C., & Milan, S. E. (2012). The IMF dependence of the local time of transpolar arcs: Implications for formation mechanism. *Journal of Geophysical Research*, *117*, A03213. https://doi.org/10.1029/2011JA017209

Grocott, A., Badman, S. V., Cowley, S. W. H., Yeoman, T. K., & Cripps, P. J. (2004). The influence of IMF by on the nature of the nightside high-latitude ionospheric flow during intervals of positive IMF Bz. *Annales Geophysicae*, *22*, 1755–1764.

Grocott, A., Cowley, S. W. H., & Sigwarth, J. B. (2003). Ionospheric flow during extended intervals of northward but By-dominated IMF. *Annales Geophysicae*, *21*, 509–538. https://doi.org/10.5194/angeo-21-509-2003

Grocott, A., & Milan, S. E. (2014). The influence of IMF clock angle timescales on the morphology of ionospheric convection. *Journal of Geophysical Research: Space Physics*, *119*, 5861–5876. https://doi.org/10.1002/2014JA020136

Grocott, A., Milan, S. E., & Yeoman, T. K. (2008). Interplanetary magnetic field control of fast azimuthal flows in the nightside high-latitude ionosphere. *Geophysical Research Letters*, *35*, L08102. https://doi.org/10.1029/2008GL033545

Grocott, A., Milan, S. E., Yeoman, T. K., Sato, N., Yukimatu, A. S., & Wild, J. A. (2010). Superposed epoch analysis of the ionospheric convection evolution during substorms, IMF b_Y dependence. *Journal of Geophysical Research*, *115*, A00I06. https://doi.org/10.1029/2010JA015728

Grocott, A., Yeoman, T. K., Milan, S. E., & Cowley, S. W. H. (2005). Interhemispheric observations of the ionospheric signature of tail reconnection during IMF-northward non-substorm intervals. *Annales Geophysicae*, *23*, 1763–1770. https://doi.org/10.5194/angeo-23-1763-2005

Iijima, T., & Potemra, T. A. (1976a). The amplitude distribution of field-aligned currents at northern high latitudes observed by triad. *Journal of Geophysical Research*, *81*, 2165–2174. https://doi.org/10.1029/JA081i013p02165

Iijima, T., & Potemra, T. A. (1976b). Field-aligned currents in the dayside cusp observed by triad. *Journal of Geophysical Research*, *81*, 5971–5979. https://doi.org/10.1029/JA081i034p05971

Iijima, T., & Potemra, T. A. (1978). Large-scale characteristics of field-aligned currents associated with substorms. *Journal of Geophysical Research*, *83*, 599–615. https://doi.org/10.1029/JA083iA02p00599

Iijima, T., Potemra, T. A., & Saflekos, N. A. (1978). Field-aligned currents in the south polar cusp and their relationship to the interplanetary magnetic field. *Journal of Geophysical Research*, *83*, 5595–5603. https://doi.org/10.1029/JA083iA12p05595

Khan, H., & Cowley, S. W. H. (1999). Observations of the response time of high-latitude ionospheric convection to variations in the interplanetary magnetic field using EISCAT and IMP-8 data. *Annales Geophysicae*, *17*, 1306–1335. https://doi.org/10.1007/s00585-999-1306-8

Khurana, K. K., Walker, R. J., & Ogino, T. (1996). Magnetic convection in the presence of interplanetary magnetic field b_y: A conceptual model and simulations. *Journal of Geophysical Research*, *101*, 4907–4916.

King, J. H., & Papitashvili, N. E. (2005). Solar wind spatial scales in and comparisons of hourly wind and ACE plasma and magnetic field data. *Journal of Geophysical Research*, *110*, A02209. https://doi.org/10.1029/2004JA010804

Kullen, A., Fear, R. C., Milan, S. E., Carter, J. A., & Karlsson, T. (2015). The statistical difference between bending arcs and regular polar arcs. *Journal of Geophysical Research: Space Physics*, *120*, 10,443–10,465. https://doi.org/10.1002/2015JA021298

Lockwood, M., & Cowley, S. W. H. (1992). Ionospheric convection and the substorm cycle. In *Proceedings of the International Conference on Substorms (ICS-1)* (pp. 99–109).

Milan, S. E. (2013). Modelling Birkeland currents in the expanding/contracting polar cap paradigm. *Journal of Geophysical Research: Space Physics*, *118*, 5532–5542. https://doi.org/10.1002/jgra.50393

Milan, S. E. (2015). Sun et lumière: Solar wind-magnetosphere coupling as deduced from ionospheric flows and polar auroras. In D. Southwood, W. H. Stanley, F. R. S. Cowley, & S. Mitton (Eds.), *Magnetospheric Plasma Physics: The Impact of Jim Dungey's Research, Astrophysics and Space Science Proceedings* (Vol. 41, pp. 271). Springer. https://doi.org/10.1007/978-3-319-18359-6_2

Milan, S. E., Carter, J. A., Korth, H., & Anderson, B. J. (2015). Principal component analysis of Birkeland currents determined by the active magnetosphere and planetary electrodynamics response experiment. *Journal of Geophysical Research: Space Physics*, 120. https://doi.org/10.1002/2015JA021680

Milan, S. E., Clausen, L. B. N., Coxon, J. C., Carter, J. A., Walach, M.-T., Laundal, K., et al. (2017). Overview of solar wind-magnetosphere-ionosphere-atmosphere coupling and the generation of magnetospheric currents. *Space Science Reviews*, *206*, 547–573. https://doi.org/10.1007/s11214-017-0333-0

Milan, S. E., Gosling, J. S., & Hubert, B. (2012). Relationship between interplanetary parameters and the magnetopause reconnection rate quantified from observations of the expanding polar cap. *Journal of Geophysical Research*, *117*, A03226. https://doi.org/10.1029/2011JA017082

Milan, S. E., Grocott, A., & Hubert, B. (2010). A superposed epoch analysis of auroral evolution during substorms: Local time of onset region. *Journal of Geophysical Research*, *115*, A00104. https://doi.org/10.1029/2010JA015663

Milan, S. E., Hubert, B., & Grocott, A. (2005). Formation and motion of a transpolar arc in response to dayside and nightside reconnection. *Journal of Geophysical Research*, *110*, A01212. https://doi.org/10.1029/2004JA010835

Milan, S. E., Provan, G., & Hubert, B. (2007). Magnetic flux transport in the dungey cycle: A survey of dayside and nightside reconnection rates. *Journal of Geophysical Research*, *112*, A01209. https://doi.org/10.1029/2006JA011642

Murphy, K. R., Mann, I. R., Rae, I. J., Waters, C. L., Frey, H. U., Kale, A., et al. (2013). The detailed spatial structure of field-aligned currents comprising the substorm current wedge. *Journal of Geophysical Research: Space Physics*, *118*, 7714–7727. https://doi.org/10.1002/2013JA018979

Newell, P. T., & Gjerloev, J. W. (2011). Evaluation of superMAG auroral electrojet indices as indicators of substorms and auroral power. *Journal of Geophysical Research*, *116*, A12211. https://doi.org/10.1029/2011JA016779

Østgaard, N., Tsyganenko, N. A., Mende, S. B., Frey, H. U., Immel, T. J., Fillingim, M., et al. (2005). Observations and model predictions of substorm auroral asymmetries in the conjugate hemispheres. *Geophysical Research Letters*, *32*, L05111. https://doi.org/10.1029/2004GL022166

Pitkänen, T., Hamrin, M., Kullen, A., Maggiolo, R., Karlsson, T., Nilsson, H., & Norqvist, P. (2016). Response of magnetotail twisting to variations in IMF B_y: A THEMIS case study 1–2 january 2009. *Geophysical Research Letters*, *43*, 7822–7830. https://doi.org/10.1002/2016GL070068

Pitkänen, T., Hamrin, M., Norqvist, P., Karlsson, T., Nilsson, H., Kullen, A., et al. (2015). Azimuthal velocity shear within an earthward fast flow—Further evidence for magnetotail untwisting. *Annales Geophysicae*, *33*, 245–255. https://doi.org/10.5194/angeo-33-245-2015

Reistad, J.-P., Østgaard, N., Tenfjord, P., Laundal, K. M., Snekvik, K., Haaland, S., et al. (2016). Dynamic effects of restoring footpoint symmetry on closed magnetic field-lines. *Journal of Geophysical Research: Space Physics*, *121*, 3963–3977. https://doi.org/10.1002/2015JA022058

Rong, Z. J., Lui, A. T. Y., Wan, W. X., Yang, Y. Y., Shen, C., Petrukovich, A. A., et al. (2015). Time delay of interplanetary magnetic field penetration into Earth's magnetotail. *Journal of Geophysical Research: Space Physics*, *120*, 3406–3414. https://doi.org/10.1002/2014JA020452

Snekvik, K., Østgaard, N. P., Tenfjord, P. R., Laundal, K. M., Milan, S. E., & Haaland, S. E. (2017). Dayside and nightside magnetic field responses at 780 km altitude to dayside reconnection. *Journal of Geophysical Research: Space Physics*, 122. https://doi.org/10.1002/2016JA023177

Svalgaard, L. (1973). Polar cap magnetic variations and their relationship with the interplanetary magnetic sector structure. *Journal of Geophysical Research*, *78*, 2064.

Tenfjord, P., Østgaard, N, Strangeway R., Haaland, S., Snekvik, K., Laundal, K. M., et al. (2017). Magnetospheric response and reconfiguration times following IMF by reversals. *Journal of Geophysical Research: Space Physics*, *122*, 417–431. https://doi.org/10.1002/2016JA023018

Waters, C. L., Anderson, B. J., & Liou, K. (2001). Estimation of global field aligned currents using the iridium system magnetometer data. *Geophysical Research Letters*, *28*, 2165–2168.

Wild, J. A., Woodfield, E. E., & Morley, S. K. (2009). On the triggering of auroral substorms by northward turnings of the interplanetary magnetic field. *Annales Geophysicae*, *27*, 3559–3570. https:www.ann-geophys.net/27/3559/2009/

Wilder, F. D., Eriksson, S., Korth, H., Baker, J. B. H., Hairston, M. R., Heinselman, C., & Anderson, B. J. (2013). Field-aligned current reconfiguration and magnetospheric response to an impulse in the interplanetary magnetic field B_Y component. *Geophysical Research Letters*, *40*, 2489–2494. https://doi.org/10.1002/grl.50505